Article:

Hart, J.M., Carswell, W.D., García-Sakai, V. et al. (5 more authors) (2025) Structural and dynamic origins of Payne effect reduction by steric stabilization in silica reinforced poly(butadiene) nanocomposites. Polymer Composites. ISSN 0272-8397

https://doi.org/10.1002/pc.70163

Polymer Composites

WILEY | spe INSPIRING PLASTICS PROFESSIONALS

RESEARCH ARTICLE OPEN ACCESS

Structural and Dynamic Origins of Payne Effect Reduction by Steric Stabilization in Silica Reinforced Poly(butadiene) Nanocomposites

James M. Hart[1] | W. Douglas Carswell[1] | Victoria García-Sakai[2] | Bernhard Frick[3] | Stephen C. Boothroyd[1] | Lian R. Hutchings[1] | Nigel Clarke[4] | Richard L. Thompson[1]

[1]Department of Chemistry, Durham University, Durham, UK | [2]Science & Technology Facilities Council, ISIS Facility, Rutherford Appleton Laboratory, Didcot, UK | [3]Institut Laue-Langevin, Grenoble, France | [4]Department of Physics and Astronomy, University of Sheffield, Sheffield, UK

Correspondence: Richard L. Thompson (r.l.thompson@durham.ac.uk)

Received: 29 April 2025 | **Revised:** 16 June 2025 | **Accepted:** 2 July 2025

Funding: J.M.H. was supported by STFC via ST/L502625/1, part of the STFC Global Challenge Studentships scheme.

Keywords: neutron scattering | non-linear rheology | QENS | steric stabilization

ABSTRACT

Silica nanoparticles in polybutadiene nanocomposites cause significantly hindered polymer dynamics in the form of a glassy layer, which can extend more than 10 nm from the nanoparticle surface. We present experiments for a well-defined series of these nanocomposites to contrast the contributions of free chain ends versus hindered dynamics on the non-linear rheological effects associated with energy loss in transport. Quasi-elastic neutron scattering (QENS) experiments using isotopic labeling and interfacially-active polymers enabled quantification of the glassy layer's thickness, which we relate to the strain softening (Payne effect), energy dissipation and the previously established nanostructure of the materials. We explored the thickness of the glassy layer from near the bulk glass transition temperature up to 363 K, in the presence or absence of nanoparticles and interfacially active polymers. Although the glassy layer becomes thinner with increasing temperature, it remains significant (> 3 nm) even when the sample is more than 180 K above the bulk glass transition temperature. This layer can account for the substantial levels of reinforcement, up to a factor of 20, and energy dissipation observed in silica filled rubbers beyond values expected from particle volume fraction arguments alone. Since the interfacially-active polymers simultaneously inhibit nanoparticle aggregation and introduce polymer chain ends to the interparticle region, these experiments provide a direct test of whether energy loss in reinforced nanocomposites is attributable to “glassy bridges” between particles or chain ends. We show that while chain ends may be significant at low strain, below 1%, the percolation of the glassy layer of hindered polymer dynamics between silica particles dominates the Payne effect at high strain (~10% or more) and that this contribution can be dramatically reduced by sufficient steric stabilization to the nanoparticles.

1 | Introduction

Filled rubbers display significant non-linear reinforcement of the elastic modulus, which greatly improves material strength, but unfortunately is also associated with a strain softening phenomenon, the Payne effect [1–3]. In road transport, this effect contributes to the rolling resistance of tires, which has been attributed to 11.5% of the energy consumption of passenger cars [4]. While this effect may be valuable in some circumstances, such as viscoelastic damping in construction materials [5], it is usually regarded as undesirable. Better understanding and control of this behavior is necessary for transport, which is an important challenge area connecting to United Nations Sustainable Development goals, notably UNSDG7—Affordable and clean

---

https://doi.org/10.1002/pc.70163

Summary

- QENS reveals location and extent of hindered dynamics.
- "Glassy layer", around silica persists at $> 180\,\mathrm{K}$ above T_g of PBd.
- Energy dissipation at high strain dominated by glassy bridges.
- Energy dissipation at low strain dominated by chain ends.
- Steric stabilization introduces chain ends but disrupts glassy bridges.

energy and USDG13—Climate change [6]. These energy dissipation effects are noticeably more present in composite materials than in their constituent components; therefore, attempts to understand and control these effects naturally tend to focus on the interfaces that are created when composites are produced [7].

Interfacial interactions are reported to convey reinforcement to composite materials through several mechanisms, including trapped entanglements [8], dynamic heterogeneity [9] or the formation of a glassy layer of polymer around filler particles [10]. Others contend that reinforcement and strain softening arise from filler networking and agglomeration [11–13]. These concepts are not mutually exclusive; indeed, the glassy layer may provide pathways for filler network formation in the composite, Figure 1a [11]. However, it has also been proposed that energy dissipation is due to frictional losses associated with chain ends [14]. Here, we present experiments to explore and resolve these possibilities by using steric stabilization to silica nanoparticles in a series of model nanocomposites to enhance nanoparticle separation while simultaneously adding polymer chain ends to the inter-particle region where strain is amplified. As well as investigating the non-linear rheology for these nanocomposites, we use deuterium labeling and quasi-elastic neutron scattering (QENS) to determine the range of influence of the nanoparticle filler on the polymer dynamics.

The application of QENS to study polymer dynamics in nanocomposites has emerged as a valuable tool [15, 16], notably, with the possibility of using isotopic labeling to isolate the dynamics of similar components in these complex materials [15, 17–19]. The technique of QENS measures the energy transferred between scattered neutrons and atomic nuclei in a sample, providing direct characterization of their dynamics. Studies using this method by Akcora et al. found an inhibited surface layer on PMMA grafted silica composites [20]. More recently, evidence for significantly hindered dynamics was reported for polymers with attractive interactions to nanoparticles by Bailey et al. [21, 22] and Wagner et al. [23] The dynamics of polymer chains at interfaces is an area of considerable interest in its own right and has been explored using dielectric spectroscopy, NMR, bulk thermal analysis and rheology [24–26]. Authors have reported either slowed or accelerated dynamics at interfaces depending on the particular system and experimental range studied [27]. Separate neutron spin echo experiments confirm that translational motions of polymer chains are inhibited with the addition of nanoparticles [28–30]. These and other related methodologies are reviewed in detail elsewhere [18, 31].

We have previously shown that tetrahydroxy-end-functional interfacially-active polybutadienes, "4OH-PBd" are highly effective dispersing agents for silica nanoparticles in a perdeuterated polybutadiene (d_6-PBd) matrix [32, 33]. SANS experiments revealed the spontaneous formation of a steric stabilizing layer of 4OH-PBd at the silica nanoparticle interface and dramatic reduction to the correlation length of silica aggregates, illustrated schematically Figure 1b. In the concentration range of 4OH-PBd-xk studied here, the grafting density is sufficiently high to ensure well-dispersed silica nanoparticles. We also established with linear rheology that the silica network that contributes to the elastic modulus at low frequency is disrupted by the end-functional polymer [33]. The dispersion of nanoparticles may be important in mitigating for strain softening (Payne effect), particularly in the case of silica fillers, which can have significantly nonlinear rheology arising from agglomeration [3]. These interfacially-active polybutadienes become strongly tethered to silica surfaces by their OH groups (sticking energy approximately 9–10 k_BT) [32], and partition almost exclusively to silica interfaces in thin films [33]. While it might be expected that dense adsorbed brush layers could result in autophobic dewetting [34] of the d_6-PBd matrix, we did not observe this effect in our SANS studies. We believe that this is because the adsorbed layer is insufficiently dense to fully exclude the matrix homopolymer because the normalized grafting density is lower than in the cases where autophobic dewetting has

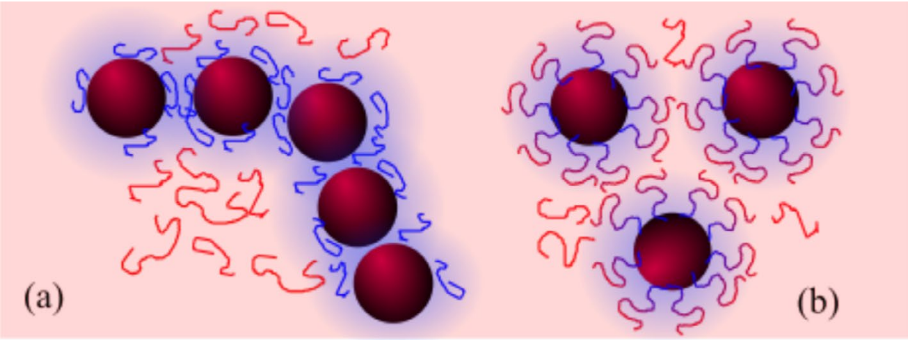

FIGURE 1 | Schematic of silica nanoparticles (dark red spheres) in a polymer nanocomposite. The blue halo illustrates an interfacial layer of glassy polymer, which percolates between bare nanoparticles (a) but could be separated into discrete domains by sufficient steric stabilization (b). The steric stabilization process, however, does introduce more chain-ends to the interstitial space between the nanoparticles.

been found. This interpretation was supported by the presence of Debye-like scattering in our SANS experiments which strongly suggests an appreciable degree of mixing between the adsorbed 4OH-PBd chains and the free d_6-PBd chains. Similar behavior was also reported by Phillipe et al. as evidence for chain mixing of H/D polymers in the presence of silica nanoparticles [19].

Here, we exploit this behavior, and the unique ability of QENS with H/D labeling [15, 35] to highlight the dynamics of the polymer near the silica surface [21]. We quantify the temperature dependent thickness of the glassy layer present around nanoparticles and consider these results in the context of non-linear rheology of the same materials.

2 | Experimental

2.1 | Materials

The synthesis and characterization of the tetrahydroxyl end functionalized polybutadiene "4OH-PBd-*X*k", where *X* is the approximate molecular weight in kg/mol, have been reported in detail previously [32]. Silica nanospheres of average hydrodynamic radius 51 ± 6 nm were produced using the Stöber process [36]. Non-functionalised hydrogenous (M_n: 136 kg/mol, M_w: 280 kg/mol, dispersity $Đ$: 2.07, "PBd-280 k") and perdeuterated (d_6) polybutadiene (M_n: 130 kg/mol M_w: 138 kg/mol $Đ$: 1.06, "d_6-PBd-140 k") of primarily 1,4 addition were purchased from Sigma Aldrich (UK) and Polymer Source (Canada), respectively, and used as received. All sample components were dispersed together in dichloromethane, sonicated to ensure good dispersion of the nanospheres, solvent cast, and thoroughly dried.

2.2 | Non-Linear Rheology

Composites containing PBd-280 k, 4OH-PBd-15 k, and Stöber silica were subjected to oscillatory strain tests with an AR2000 rheometer; the oscillation frequency was 1 Hz and the strain was varied between 0.01% and30%. We used a similar methodology to that established elsewhere to study the viscoelastic properties of polymer composites [37–40]. The samples (8 mm diameter, 1 mm thick) were divided into two sets; the first composite set did not contain the end-functionalised polybutadiene, while in the second set a 50:50 blend of PBd-280 k and 4OH-PBd-15 k was the polymer matrix. A series of Stöber silica loadings were investigated in both sets.

2.3 | Differential Scanning Calorimetry

Differential scanning calorimetry (DSC) measurements were performed using a Perkin Elmer DSC 8000 equipped with liquid nitrogen cooling to determine the calorimetric values of the glass transition temperature for composite and blend samples [41]. Approximately 10 mg of sample was weighed into a DSC pan and cooled to −120°C. After a 2-min isotherm, samples were heated at 10°C/min from −120°C to 20°C, and the T_g values were calculated from the midpoint of the step in heat flow using Pyris 13.2.1.0007 software.

2.4 | QENS Sample Preparation

Samples were formed into 65 × 35 × 0.1 mm sheets using an IR sample press. Because QENS experiments over a range of temperatures require long acquisition times, a limited range of samples were selected, and their details are summarized in Table 1. Two control samples with "no silica" were necessary to isolate the impact of silica nanoparticles on the PBd and 4OH-PBd dynamics. "PBd-280 k" and "4OH-PBd-15 k: d_6-PBd-140 k" were compared to establish that blending hydrogenous and deuterated polybutadiene had no effect on the dynamics of hydrogenous polymer.

In addition to the two "no silica" controls, three composite samples were also prepared and can be classified as sketched in Figure 1a,b. Stabilized composite samples contained 50:30:20 (w/w) silica: d_6-PBd-140 k:4OH-PBd of either 10 or 15 k in weight. A fully hydrogenous composite sample of 50:50 (w/w) silica: PBd-280 k was also formed, in which the PBd is not exclusively located adjacent to the silica nanoparticles. Having some deuterated unfunctionalised d_6-PBd also present in the 4OH-PBd-*X*k composite samples ensures that the functional polymer can locate almost exclusively at the silica interfaces.

TABLE 1 | Summary of composition of samples prepared for QENS experiments.

Sample name (class)	DSC T_g/°C	[silica]/wt%	[d_6-PBd]/wt%	[hPBd]/wt%	IRIS temp/K	IN16B temp/K
PBd-280 k (no silica)	−96.7	0	0	100	5, 220, 250, 280, 310, 363	—
4OH-PBd-15 k:d_6-PBd-140 k (no silica)	−96.5	0	50	50	5, 220, 250, 280, 310, 363	5, 220, 250, 280, 310, 363
PBd-280 k composite (composite)	−96.5	50	0	50	5, 220, 250, 280, 310, 363	220, 250, 280, 310, 363
4OH-PBd-15 k composite (composite)	−98.2	50	30	20	5, 220, 250, 280, 310, 363	220, 250, 280, 310, 363
4OH-PBd-10 k composite (composite)	−99.4	50	30	20	5, 310, 363	—

Crucially, comparison of "4OH-PBd-15 k:d_6-PBd-140 k" with "4OH-PBd-15 k composite" isolates the effect of silica on the dynamics of the end functional 4OH-PBd materials. The compositions were chosen to enable these features to be isolated, while maintaining sufficient hydrogenous material in the samples to obtain a strong QENS signal that was dominated by the hydrogenous PBd component. Note that 50% w/w silica in QENS samples is 26% ± 1% silica v/v.

2.5 | QENS Experiments

QENS experiments were carried out on the IRIS [42] (STFC Rutherford Appleton Laboratories, Harwell Oxford, UK) and IN16b [43] (Institute Laue Langevin, Grenoble, France) spectrometers. The IRIS spectrometer, with PG002 analyzer, yields an energy transfer range of ±0.4 meV with a resolution of 17.5 μeV. The IN16B spectrometer at the Institute Laue Langevin, Grenoble, France, was used with "unpolished" Si(111) monochromators and analyzers to measure over an energy transfer range of ±31 μeV with 0.75 μeV FWHM resolution. On IRIS, the use of the graphite 002 analyzer yields an observation timescale of dynamics up to 150 ps and a Q range of 0.42–1.85 Å^{-1}, where Q is the scattering vector. On IN16B, the setup enables the observation of processes on timescales up to approximately 4 ns and a Q range of 0.2–1.8 Å^{-1}. Sample sheets were inserted into standard annular aluminum cans for each spectrometer. Data were collected on both instruments at temperatures between 220 and 363 K. These provided a spectrum of dynamics measurements ranging from near T_g to the maximum operational temperatures of tyre materials. Due to time constraints, 4OH-PBd-10 k composite runs were performed only at 310 and 363 K. A subset of these samples were examined on IN16B. A baseline at 5 K was run for each sample on IRIS, and on IN16B a baseline of the blend sample was taken. LAMP [44] software was used for data reduction in IN16B. Mantid software [45] was used for data reduction on IRIS and for fast Fourier transforming the quasi-elastic scattering peaks to $I(Q, t)$.

3 | Results

3.1 | Thermal Analysis

DSC analysis showed that the glass transition temperature of the PBd-based QENS samples was relatively independent of the PB functionalization or the presence of silica, Table 1. DSC thermograms are provided in Supporting Information S1. Although the presence of nanoparticles can have a significant impact on T_g, depending on the chemistry and interactions of the polymer and the nanoparticle [46], we saw little evidence for this effect in our materials. All of the calorimetric T_gs were in the range −98.0°C ± 1.5°C (~175 K), with no strong dependence on the presence of silica, functionalization, or deuteration. The calorimetric T_g of polybutadiene is well established to be sensitive to the proportion of *trans*, *cis*, and particularly *vinyl* units in the polymer chain microstructure [47]. The variations in T_g, which are small compared to the temperature range of interest for this work, are likely to arise mainly from variations in polymer chain microstructure.

3.2 | Rheology

The influences of steric stabilization and nanoparticle loading on non-linear rheology are shown in Figure 2, normalized to the limit of linear behavior at low strain. Absolute values for the volume fraction dependence of G' in the limit of low strain indicate

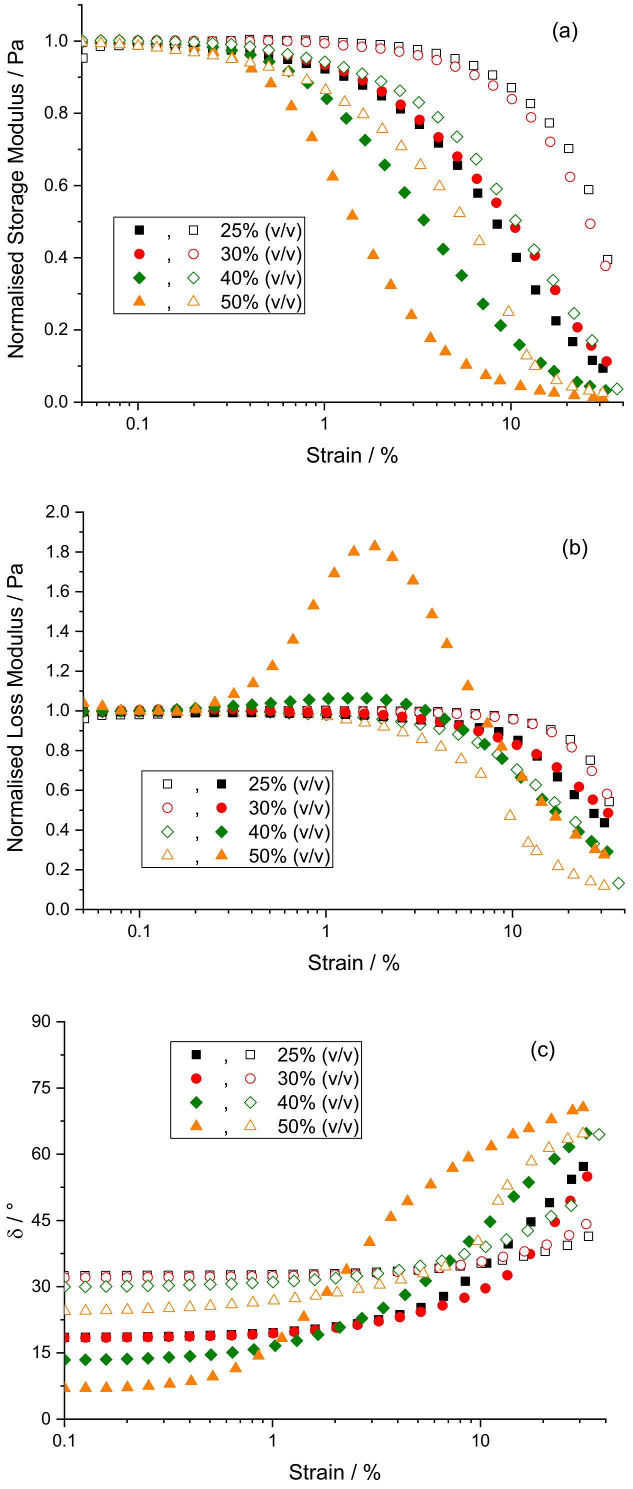

FIGURE 2 | Strain dependence of normalized (a) storage modulus, (b) loss modulus, and (c) phase angle for PBd composites, with 25, 30, 40, 50% (v/v) silica nanoparticles. Data for composites in a pure PBd280k matrix are shown as solid points and for (1:1 4OH-PBd-15 k:PBd280k) matrix as hollow points.

reinforcement exceeds the prediction of a simple Guth-Gold theory by an order of magnitude are presented in Supporting Information S2. In every sample, there is a plateau region of linear behavior, before the onset of strain softening, Figure 2a, which is qualitatively similar to other filled rubber composites. The linear viscoelastic range decreases with increasing silica loading, but is significantly extended by the presence of 4OH-PBd-15 k. The peak in loss modulus, Figure 2b coincides with the early onset of strain softening and is typically attributed to the breakdown of an agglomerated structure, as reported elsewhere [37–39]. Here, the long-range structure is suppressed in the composites containing 4OH-PBd-15 k, which keeps the nanoparticles dispersed, hence the loss peak is reduced or absent in these samples. Here we note that the loss peak increases dramatically at the highest loading, which presumably corresponds to a concentration at which some form of rigid network percolates through much of the sample. The delayed onset of strain softening in the samples containing 4OH-PBd-15 k is clearly apparent from the strain-dependence of the phase angle, δ, shown in Figure 2c, where

$$\tan\delta = G' / G'' \tag{1}$$

3.3 | QENS

Representative QENS spectra for the 4OH-PBd-15 k:d$_6$-PBd-140 k blend, PBd-280 k composite and 4OH-PBd-15 k composite samples from IRIS and IN16b are shown in Figure 3. The scattering signal from each sample is dominated by the incoherent contribution from the hydrogenous components. (Scattering cross-sections are given in Table S1) For both instruments, there is a clear trend from slow to fast dynamics in the order 4OH-PBd-15 k composite < PBd-280 k composite < blend, as seen from the increased peak width. The fastest dynamics are found for the sample which contains no silica. Intermediate dynamics are found when there is silica, but the hydrogenous PBd-280 k is not functionalized; therefore is not located specifically at the silica interface. The slowest dynamics occur when the hydrogenous polymer, 4OH-PBd-15 k is present and is located at the interface of the silica nanoparticles [33].

All QENS spectra were fast Fourier transformed to produce decaying intermediate scattering functions. These decays were fitted to a Kohlrausch–Williams–Watts (KWW) stretched exponential function of the form,

$$I(Q,t) = A + (1-A)e^{(-t/\tau)^{\beta}} \tag{2}$$

where A is the background, τ is the characteristic decay time, and β is the stretching exponent. The background, A, arises from the portion of the material that does not relax over the instrumental timescale and so depends on which spectrometer is used in each experiment.

The decay time, τ, is an average characteristic time for the overall relaxation rate of the matrix, and β can be interpreted as a measure of the dynamic heterogeneity (distribution of rates), where $\beta = 1$ implies a single homogeneous relaxation rate. For polymer systems β is usually independent of temperature and Q [48], and takes values between 0.4 and 0.6 [49, 50].

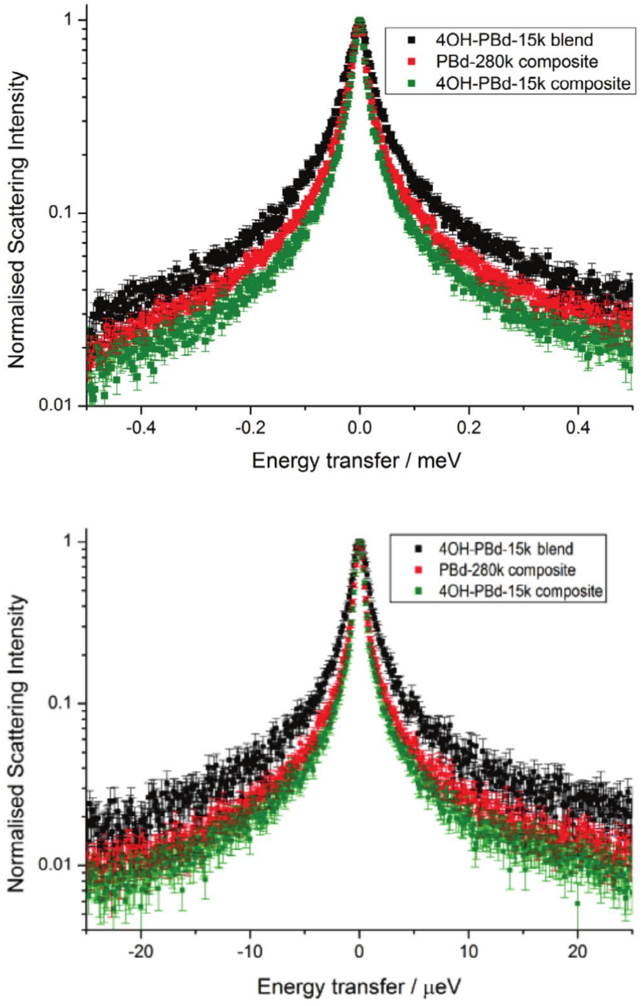

FIGURE 3 | Normalized scattering intensity (top) from IRIS for selected samples at 363 K, $Q = 1.27\,\text{Å}^{-1}$, and (bottom) IN16B energy transfer peaks for selected samples, temperature = 280 K, $Q = 1.23\,\text{Å}^{-1}$. The data highlight the influence of silica on the dynamics of functionalized and unfunctionalized PBd compared to the blend.

Initial fitting was performed to determine the stretching exponent, β, which was constrained between 0 and 1 to prevent unphysical fits. An average of β values was taken for each sample and used as a fixed parameter for a second iteration of fitting, which was necessary to avoid overparameterisation [49]. All of the $I(Q, t)$ data could be well fitted for each instrument separately using Equation (2), Figure 4. A scaling factor (Figure S3) was necessary to obtain overlapping data with a continuously decaying $I(Q, t)$ for both instruments, Figure 5. The Q-dependence of this factor follows Debye-Waller behavior and is likely to arise because some of the faster dynamics measured on IRIS are too energetic for IN16B to detect at short timescales. For this reason the IN16B data was scaled with respect to the IRIS data, which characterizes the intermediate scattering function in the limit of $t \rightarrow 0$ more accurately. It was not possible to fit $I(Q, t)$ for the combined data over the full dynamic range from 0.005 to 3.5 ns consistently with a single stretched exponential (Figure 5, see also Figure S3). This is likely to arise because the instruments are sensitive to different modes of motion on their respective timescales. Over the temperature range of our experiments, 220 to 363 K, the τ_α and τ_β relaxations of polybutadiene are expected

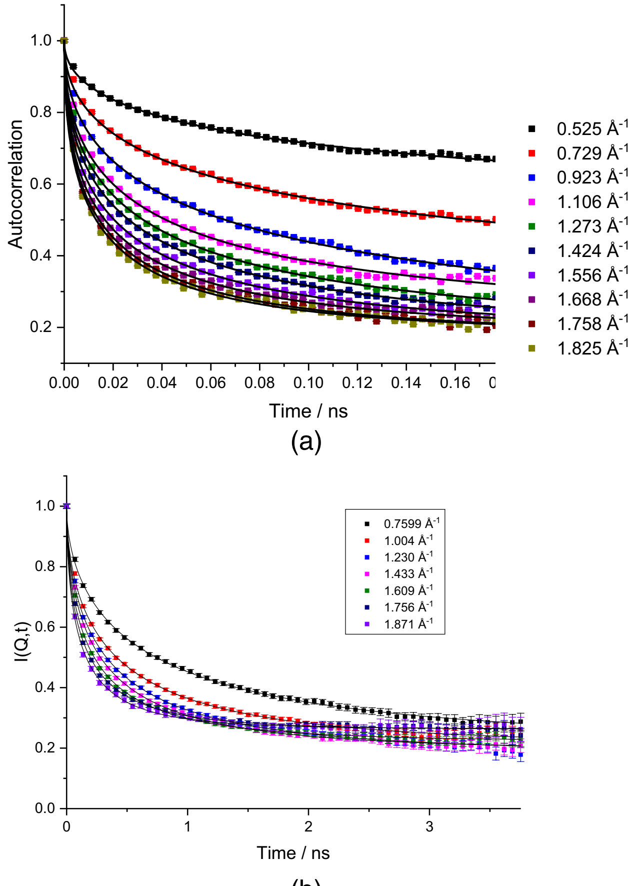

(a)

(b)

FIGURE 4 | (a) Intermediate scattering functions, $I(Q, t)$ measured on IRIS, lines are fitted stretched exponential functions, 4OH-PBd-15k composite at 310 K. (b) Intermediate scattering functions measured on IN16B, lines are fitted stretched exponential functions, 4OH-PBd-15k composite at 280 K.

to occur on a timescale of approximately 0.05 and 0.005 ps respectively [51], which are largely within the range of IRIS but largely out of the range of IN16b. On the other hand, IN16b is sensitive to slower dynamic processes that have no signature in the energy transfer range that can be detected using IRIS. Results for IRIS and IN16B (scaled w.r.t. IRIS) are therefore analyzed separately.

Derived values for τ and β (Figure S4, tabulated values are available [52]) show little systematic variation between the samples, indicating that the major distinction in dynamics arises from the portion of "mobile" protons, and not from increased heterogeneity.

When silica nanoparticles are included in the matrix, A is significantly increased with respect to the unfilled polymer blends. Data are included in Figures S5 and S6 for IRIS and IN16B respectively. The silica immobilizes some fraction of the polymer in composite samples, by a much greater amount than could be accounted for by its coherent scattering contribution. Remarkably, even over the much longer timescale of IN16B, a significant proportion of the hydrogenous polymer remains immobile well above the calorimetric T_g (175 K). The only exception to this observation is at low Q on IRIS where the data are noisy, presumably because inherently slow PBd dynamics on the larger length scales implied by low Q are not readily detected within the range of this spectrometer.

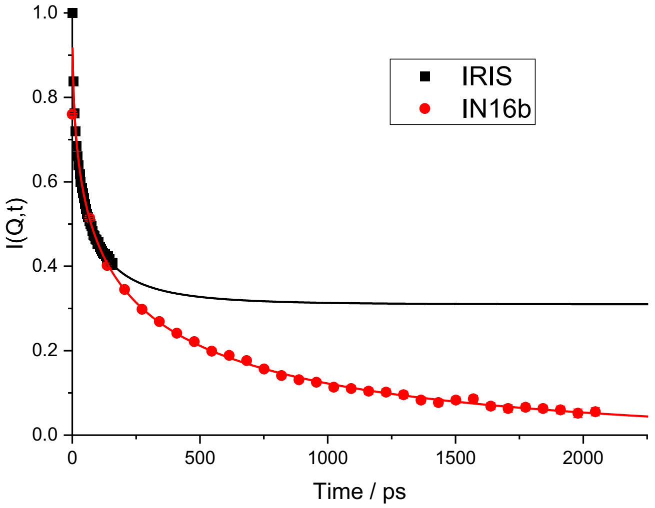

FIGURE 5 | Comparison of IN16B and IRIS intermediate scattering functions with scaling, lines are fitted stretched exponential functions, 4OHPBd-15k d_6-dPB 140k blend, 280 K, Q: 1.23 Å^{-1}.

4 | Discussion

4.1 | Range of Influence of Silica Nanoparticles on Polymer Dynamics

We have previously shown with SANS and linear rheology that 4OH-PBd-*X*k brush layers can adsorb efficiently to silica nanoparticles, providing steric stabilization in nanocomposites and disrupting silica networks [33]. This structural detail underpins the interpretation of the dynamics proposed in schematic form in Figure 1. In the blend there is no silica to alter the dynamics. In the composite, in the absence of 4OH-PBd-*X*k, Figure 1a, the hydrogenous polymer is present in a mixture of environments, "adjacent to" or "remote from" the silica. In the composite samples including silica, d_6-PBd-140 k and 4OH-PBd-*X*k, Figure 1b, adsorption ensures that the 4OH-PBd-*X*k which is the only hydrogenous polymer is "adjacent to" the silica. The order of increasingly hindered dynamics (Figure 3) is consistent with this effect being caused by silica and being most significant for polymer chains adjacent to silica.

We calculate the spatial extent of the inhibited layer by assuming that at the silica NP/polymer interface, $A = 1$ and treat the polymer as immobile within the timescale accessible on the QENS experiment. Given that a significant background value was measured, even on the IN16B experiments, this assumption is certainly reasonable. An additional boundary is provided by the background value in the absence of silica, A_{blend}. This value defines the immobile fraction at a very large distance from any particle surface. We now define $D(x)$ as the fraction of "immobile" material, which is initially assumed to decay exponentially with distance, x, from each nanoparticle surface,

$$D(x) = A_{\text{blend}} + \left(1 - A_{\text{blend}}\right)e^{-x/d} \tag{3}$$

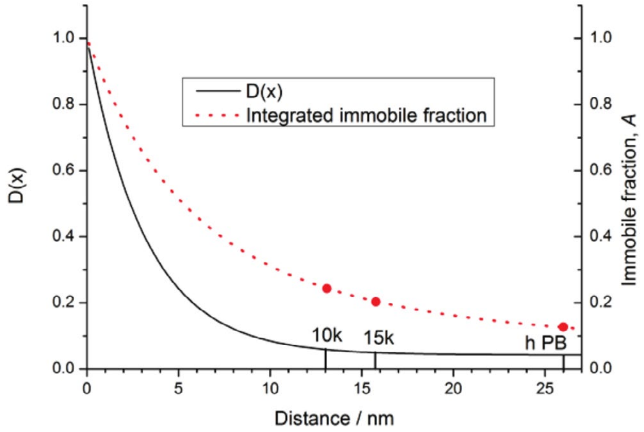

FIGURE 6 | Calculated and volume average KWW background in relation to distance from silica surface, up to the limit of integration, $x = 26\,\text{nm}$.

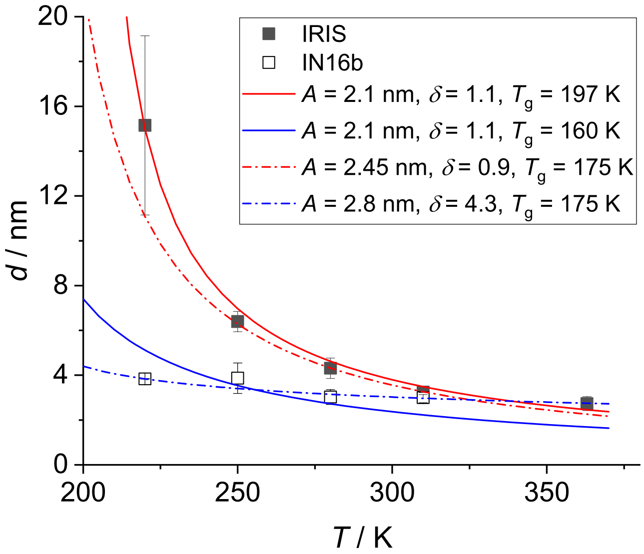

FIGURE 7 | Characteristic length for the immobile layer adjacent to silica interface, IRIS (full) and scaled IN16B (hollow) and fits to Equation (6).

where d is the characteristic spatial decay length. The spatial extent of the hindered dynamics, defined by d, is obtained correctly when $D(x)$ gives the correct measured value for A, which is the average over the entire sample volume. To do this, $D(x)$ must be integrated over appropriate limits. The lower limit, x_{min}, is the silica nanoparticle radius, and the upper limit is either the thickness of the adsorbed 4OH-PBd-Xk polymer, if present, or half the average separation of the silica particles. Our previous SANS experiments established the thickness to be 13.0 and 15.7 nm for 4OH-PBd-10 k and 4OH-PBd-15 k, respectively [33]. In the case of the hPBd composite, the upper integration limit was defined by half the calculated lattice parameter of the notional FCC unit minus the particle radius, yielding 26 nm. The remaining volume (i.e., the interstitial region not covered by the FCC spheres) was treated as having the neat polymer background value and incorporated into the calculation of the average background value. Although this distribution is clearly imperfect (we previously measured a fractal dimension of order 2 at low [4OH-PBd-Xk] [33]), we note that as long as this value for the upper limit of integration is large and representative of the silica volume fraction, it does not introduce a large error.

Figure 6 illustrates the local dependence of $D(x)$ for typical conditions of these systems. The red curve shows the spherically integrated value of $A(x)$ as a function of the upper integration limit.

$$A(x) = \frac{1}{V(x)} \int_{x_{\text{min}}}^{x} x^2 D(x)\, \mathrm{d}x \tag{4}$$

where

$$V(x) = \int_{x_{\text{min}}}^{x} x^2\, \mathrm{d}x \tag{5}$$

From the known thickness values of functional 4OH-PBd-*X*k adsorbed layers, the limits for the integral were defined. This is an acceptable approximation since the deuterated bulk does not greatly contribute to the incoherent scattering of the system (Table S1) [32].

With a single value of d, distinct A values are calculated for 4OH-PBd-10 k and 4OH-PBd-15 k due to the different integration limits. This calculation is reversible, and d can be determined by comparing and fitting the calculated background values to those measured by the QENS instrument, Figure S7. The close agreement found between the calculated and experimental values suggests the simple model gives a reliable measure of the dynamics of the glassy layer. The main discrepancies between calculation and measurement are at 220 and 363 K, with the 4OH-PBd-15 k and fully hydrogenated samples, respectively. These samples correspond to the extremes of dynamic range for the system, that is, lowest temperature in combination with the hydrogenous material being confined to the silica interface region, or highest temperature and no silica present. These discrepancies are likely to arise from the limits of the IRIS spectrometer, as relaxations outside the range of 4–150 ps, in this case close to T_g or over 180 K above T_g, are difficult to measure accurately.

The general trend of decreasing d with increasing temperature is consistent with the glassy layer being thinner as the temperature is increased to be well above T_g. If the Payne effect can be ascribed to glassy bridges [11], then it would be reasonable to expect that this effect also decreases with increasing temperature. In this respect, our results are consistent with the temperature-dependent results of Luo et al. and Warasitthinon et al., who reported that the Payne effect is less evident with increasing temperature [53, 54].

The scaled IN16b data were analyzed in a similar way. The behavior is consistent, but systematically shifted to lower d values because a greater proportion of material can relax on the longer timescale characterized by this instrument (Figure 7). Qualitatively, the presence of an increased background for composites at these greater timescales lends support to the treatment of the silica–PBd interface as immobile.

Figure 7 shows that, particularly for the shorter timescales measured on IRIS, the apparent thickness of the immobile layer surrounding the silica nanoparticles begins to diverge as the temperature decreases toward the bulk T_g, 175 K.

The thickness dependence of the immobile layer can be quite well described for each instrument by Equation (6), which is adapted from the work of Keddie et al. on thin films, allowing for the T_g increasing at the buried silica interface rather than decreasing at an exposed air surface [55].

$$d(T) = \frac{C}{\left(\frac{T}{T_g} - 1\right)^{1/\delta}} \tag{6}$$

where the fitted parameters, C and δ, which describe the length scale and shape of spatially dependent glass transition were significantly different for each spectrometer when the value of T_g was constrained to the calorimetric value, 175 K. By allowing the T_g value to vary between instruments it was possible to simultaneously fit both sets of data, but the quality of fit was significantly poorer and the floated T_g values ranged from well-above to well-below the calorimetric value, which seems physically unreasonable. Regardless of the fit to Equation (6), it is remarkable and unambiguous that for both QENS experiments, the characteristic range of hindered motion is significant (of the order 3 nm) even at 180 K above T_g.

4.2 | Nanoscale Structure and Macroscopic Properties of Nanocomposites

The peak observed in the loss modulus with a strain sweep is thought to arise from energy dissipation for the breakage of network contacts [56]. Merabia et al. proposed that reinforcement and the strain softening resulted from glassy matrix bridges aiding in filler networking [11]. From previous SANS experiments, we found that the grafting density for the formation of a brush layer coincided with the onset in the dispersion of filler aggregates through steric stabilization [33]. We note also that this is consistent with the work of Genix et al., who reported that grafting on silica nanoparticles could effectively screen the slowing of dynamics that would be expected for bare nanoparticles [57]. Although it has been reported that the formation of a brush layer itself hinders dynamics [58, 59], this behavior appears to be significant only for dense polymer brushes at higher normalized grafting densities than are encountered in this work. We have carried out separate QENS experiments on crosslinked PBd networks under uniaxial strain. Samples were cross-linked versions of the 4OH-PBd-15 k/d_6-PBd blend, the PBd280k composite, and the 4OH-PBd-15 k composite, Table S2. The experimental setup is shown in Figure S8, and results for the influence of imposed strain on dynamics are summarized in Figure 8. The data for the immobile fraction measured on IRIS in this crosslinked sample are consistent with the trends for the uncrosslinked material: the dynamics of the hydrogenous PBd are hindered by the presence of silica, and this hindrance is greater when the hydrogenous PBd is confined to the region adjacent to the silica interface. Furthermore, these experiments show no discernible effect of stretching on chain dynamics in the timescale of ps. We therefore conclude that the dynamic effects observed for polymers are dominated by their proximity to the silica interface rather than from any chain stretching that arises from the adsorption of 4OH-PB-xk to this interface.

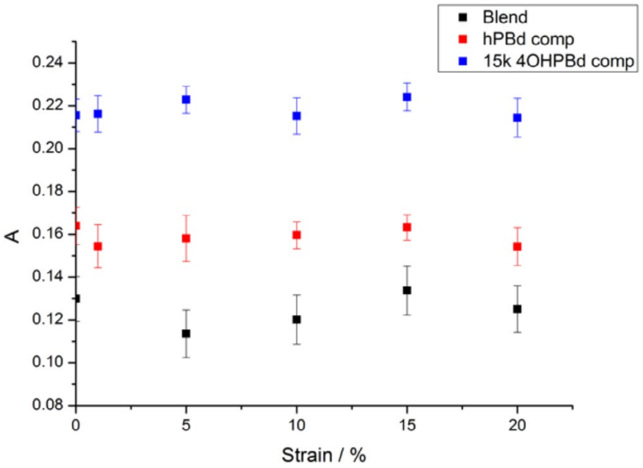

FIGURE 8 | Strain dependence of A for cross-linked analogs of PBd blends and nanocomposites studied in the present work.

Finally, we consider the thickness of the glassy layer at ambient temperature in relation to the thickness of the tethered brush layer of 4OH-PBd-15 k. At 293 K, the dynamics of the ends of the 4OH-PBd-15 k polymer brush layer, which at 15.7 nm thick exceeds the immobile layer thickness by a factor of four, should approach bulk behavior. Therefore, the steric repulsion offered by the 4OH-PBd should prevent the formation of the glassy bridges between nanoparticles. The increasing inhibition of strain softening and disappearance of the loss peak in Figure 2, for all compositions that include 4OH-PBd-15 k, shows that the Payne effect for these materials is determined by glassy layers around silica more than polymer chain ends. It is interesting to note that at low strain, the phase angle seen in Figure 2c is typically lower for the nanocomposites without the 4OH-PBd-15 k. This observation, albeit limited to shear strains of less than circa 1%, does support the point that the introduction of more chain ends to a nanocomposite can contribute to energy dissipation. However, at higher strains, > 10%, the trend is reversed, and the end functional polymer helps to reduce energy dissipation.

5 | Conclusions

We have explored the relationship between nonlinear rheology and polymer dynamics in a well-defined series of model nanocomposites. The composites were designed to identify the influence of silica nanoparticles on polymer dynamics and further how this influence changes when the interparticle separation and number of free chain ends are simultaneously increased. Hindered segmental dynamics extending a few nm from the nanoparticle/polymer interface was established and is in general agreement with measurements on different polymer nanocomposite systems [30]. The thickness of this layer is dependent on temperature, but remains significant, even at relevant operational temperatures for filled rubbers in tires, which may be more than 180 K above the bulk T_g.

The loss peak observed in strain softening rheological measurements decreased with the presence of an end-functional polybutadiene in the matrix. Suppression of strain softening and energy dissipation was determined to arise from the prevention of particle contacts with a sterically stabilizing polymer brush. Knowledge of the polymer brush thickness from QENS on labeled nanocomposites provides insight into the nature of these contacts. Our results strongly support the glassy bridging model put forward by Merabia when applied to high surface energy nanoparticles such as silica. Furthermore, the introduction of chain ends to the interparticle region does not appear to contribute significantly to energy dissipation under solicitation except at very low strain amplitudes. Finally, when considering strategies to minimize energy loss in filled rubber materials such as tires, our work highlights the need for steric stabilization of filler particles on an appropriate length scale of 2–20 nm.

Author Contributions

The manuscript was written by J.M.H. and R.L.T. through contributions of all authors. The original project plan was conceived by R.L.T., N.C., and V.G.-S. L.R.H. provided the functional polymers, and W.D.C. carried out the thermal analysis. J.M.H. carried out all experiments and analyses with support from S.C.B. (rheology) V.G.-S., and B.F. (QENS).

Acknowledgments

We thank STFC for access to neutron scattering facilities at ISIS (RB1510168 and RB1520211) and ILL. The original data is accessible via datacite: For IRIS: https://doi.org/10.5286/isis.e.58446441 and https://doi.org/10.5286/isis.e.67769287; for IN16b: https://doi.org/10.5291/ILL-DATA.9-12-443.

Conflicts of Interest

The authors declare no conflicts of interest.

Data Availability Statement

Data presented are available via Durham University collections (open access doi: https://doi.org/10.15128/r1hx11xf24k).

References

1. A. R. Payne, “A Note on the Existence of a Yield Point in the Dynamic Modulus of Loaded Vulcanizates,” *Journal of Applied Polymer Science* 3, no. 7 (1960): 127, https://doi.org/10.1002/app.1960.070030721.

2. A. P. Meera, S. Said, Y. Grohens, and S. Thomas, “Nonlinear Viscoelastic Behavior of Silica-Filled Natural Rubber Nanocomposites,” *Journal of Physical Chemistry C* 113, no. 42 (2009): 17997–18002, https://doi.org/10.1021/jp9020118.

3. Z.-Y. Li, Y.-H. Song, and Q. Zheng, “Payne Effect and Weak Overshoot in Rubber Nanocomposites,” *Chinese Journal of Polymer Science* 40, no. 1 (2022): 85–92, https://doi.org/10.1007/s10118-021-2643-7.

4. K. Holmberg, P. Andersson, and A. Erdemir, “Global Energy Consumption due to Friction in Passenger Cars,” *Tribology International* 47 (2012): 221–234, https://doi.org/10.1016/j.triboint.2011.11.022.

5. B. Yin, X. Jiao, H. Wen, Y. Li, and M. Li, “Effect of Prestrain on Payne Effect and Hysteresis Loss of Carbon-Black-Filled Rubber Vulcanizates: Measurements and Modeling,” *Polymers* 16, no. 3 (2024): 436, https://doi.org/10.3390/polym16030436.

6. United Nations Department of Economic and Social Affairs - Sustainable Development, “United Nations,” accessed April 1, 2025, https://sdgs.uk.org/goals.

7. M. Viktorova, R. Hentschke, F. Fleck, F. Taherian, and H. A. Karimi-Varzaneh, “Simulation of Elastomer Nanocomposites: Interfacial Stresses and Strains Related to Filler Dispersion, Global Deformation and the Payne Effect,” *Computational Materials Science* 223 (2023): 112144, https://doi.org/10.1016/j.commatsci.2023.112144.

8. S. S. Sternstein and A.-J. Zhu, “Reinforcement Mechanism of Nanofilled Polymer Melts as Elucidated by Nonlinear Viscoelastic Behavior,” *Macromolecules* 35, no. 19 (2002): 7262–7273, https://doi.org/10.1021/ma020482u.

9. S. Yang and P. Akcora, “Deformation of Chemically Heterogeneous Interfacial Layers of Polymer Nanocomposites,” *ACS Macro Letters* 8, no. 12 (2019): 1635–1641, https://doi.org/10.1021/acsmacrolett.9b00821.

10. G. P. Baeza, C. Dessi, S. Costanzo, et al., “Network Dynamics in Nanofilled Polymers,” *Nature Communications* 7 (2016): 11368, https://doi.org/10.1038/ncomms11368.

11. S. Merabia, P. Sotta, and D. R. Long, “A Microscopic Model for the Reinforcement and the Nonlinear Behavior of Filled Elastomers and Thermoplastic Elastomers (Payne and Mullins Effects),” *Macromolecules* 41, no. 21 (2008): 8252–8266, https://doi.org/10.1021/ma8014728.

12. A. Papon, S. Merabia, L. Guy, et al., “Unique Nonlinear Behavior of Nano-Filled Elastomers: From the Onset of Strain Softening to Large Amplitude Shear Deformations,” *Macromolecules* 45, no. 6 (2012): 2891–2904, https://doi.org/10.1021/ma202278e.

13. L. Yang, S. Huang, F. Wu, et al., “New Insights Into the Elasticity and Multi-Level Relaxation of Filler Network With Studies on the Rheology of Isotactic Polypropylene/Carbon Black Nanocomposite,” *RSC Advances* 5, no. 81 (2015): 65874–65883, https://doi.org/10.1039/C5RA10516A.

14. L. Wang, S. Zhao, A. Li, and X. Zhang, “Study on the Structure and Properties of SSBR With Large-Volume Functional Groups at the End of Chains,” *Polymer* 51, no. 9 (2010): 2084–2090, https://doi.org/10.1016/j.polymer.2010.03.006.

15. J. Maiz, E. Verde-Sesto, I. Asenjo-Sanz, et al., “Disentangling Component Dynamics in an All-Polymer Nanocomposite Based on Single-Chain Nanoparticles by Quasielastic Neutron Scattering,” *Macromolecules* 55, no. 6 (2022): 2320–2332, https://doi.org/10.1021/acs.macromol.1c02382.

16. E. Senses, A. Faraone, and P. Akcora, “Microscopic Chain Motion in Polymer Nanocomposites With Dynamically Asymmetric Interphases,” *Scientific Reports* 6, no. 1 (2016): 29326, https://doi.org/10.1038/srep29326.

17. E. J. Bailey, M. Tyagi, and K. I. Winey, “Correlation Between Backbone and Pyridine Dynamics in Poly(2-Vinyl Pyridine)/silica Polymer Nanocomposites,” *Journal of Polymer Science* 58, no. 20 (2020): 2906–2913, https://doi.org/10.1002/pol.20200416.

18. A. Swain, N. Das, V. G. Sakai, and J. Basu, “Microscopic Temperature-Dependent Structural Dynamics in Polymer Nanocomposites: Role of the Graft–Matrix Chain Interfacial Entropic Effect,” *Soft Matter* 19, no. 28 (2023): 5396–5404.

19. A.-M. Philippe, C. Sill, S. Westermann, et al., “Quantifying Structure and Dynamics of Bound and Bulk Polymer in Tailor-Made Rubber-Silica Nanocomposites,” *Frontiers in Physics* 10 (2022): 1–17, https://doi.org/10.3389/fphy.2022.1023234.

20. P. Akcora, S. K. Kumar, V. García Sakai, Y. Li, B. C. Benicewicz, and L. S. Schadler, “Segmental Dynamics in PMMA-Grafted Nanoparticle Composites,” *Macromolecules* 43, no. 19 (2010): 8275–8281, https://doi.org/10.1021/ma101240j.

21. E. J. Bailey, P. J. Griffin, M. Tyagi, and K. I. Winey, “Segmental Diffusion in Attractive Polymer Nanocomposites: A Quasi-Elastic Neutron

Scattering Study," *Macromolecules* 52, no. 2 (2019): 669–678, https://doi.org/10.1021/acs.macromol.8b01716.

22. E. J. Bailey, P. J. Griffin, R. J. Composto, and K. I. Winey, "Multiscale Dynamics of Small, Attractive Nanoparticles and Entangled Polymers in Polymer Nanocomposites," *Macromolecules* 52, no. 5 (2019): 2181–2188, https://doi.org/10.1021/acs.macromol.8b02646.

23. J. Kim, B. R. Thompson, T. Tominaga, et al., "Suppression of Segmental Chain Dynamics on a Particle's Surface in Well-Dispersed Polymer Nanocomposites," *ACS Macro Letters* 13, no. 6 (2024): 720–725, https://doi.org/10.1021/acsmacrolett.4c00168.

24. A. Papon, H. Montes, M. Hanafi, F. Lequeux, L. Guy, and K. Saalwächter, "Glass-Transition Temperature Gradient in Nanocomposites: Evidence From Nuclear Magnetic Resonance and Differential Scanning Calorimetry," *Physical Review Letters* 108, no. 6 (2012): 065702.

25. A. Mujtaba, M. Keller, S. Ilisch, et al., "Mechanical Properties and Cross-Link Density of Styrene–Butadiene Model Composites Containing Fillers With Bimodal Particle Size Distribution," *Macromolecules* 45, no. 16 (2012): 6504–6515, https://doi.org/10.1021/ma300925p.

26. S. Cheng and A. P. Sokolov, "Correlation Between the Temperature Evolution of the Interfacial Region and the Growing Dynamic Cooperativity Length Scale," *Journal of Chemical Physics* 152, no. 9 (2020): 094904.

27. A. Sharma and M. Kruteva, "Towards the Polymer Nanocomposites Based on Hairy Nanoparticles," *Frontiers in Physics* 10 (2022): 1041903, https://doi.org/10.3389/fphy.2022.1041903.

28. M. Krutyeva, A. Wischnewski, M. Monkenbusch, et al., "Effect of Nanoconfinement on Polymer Dynamics: Surface Layers and Interphases," *Physical Review Letters* 110, no. 10 (2013): 108303.

29. T. Glomann, G. J. Schneider, J. Allgaier, et al., "Microscopic Dynamics of Polyethylene Glycol Chains Interacting With Silica Nanoparticles," *Physical Review Letters* 110, no. 17 (2013): 178001, https://doi.org/10.1103/PhysRevLett.110.178001.

30. A. Arbe, J. A. Pomposo, I. Asenjo-Sanz, et al., "Single Chain Dynamic Structure Factor of Linear Polymers in an All-Polymer Nano-Composite," *Macromolecules* 49, no. 6 (2016): 2354–2364, https://doi.org/10.1021/acs.macromol.5b02519.

31. R. Ashkar, "Selective Dynamics in Polymeric Materials: Insights From Quasi-Elastic Neutron Scattering Spectroscopy," *Journal of Applied Physics* 127, no. 15 (2020): 151101, https://doi.org/10.1063/1.5144243.

32. S. M. Kimani, S. J. Hardman, L. R. Hutchings, N. Clarke, and R. L. Thompson, "Synthesis and Surface Activity of High and Low Surface Energy Multi-End Functional Polybutadiene Additives," *Soft Matter* 8, no. 12 (2012): 3487–3496, https://doi.org/10.1039/C2SM07361G.

33. J. M. Hart, S. M. Kimani, L. R. Hutchings, et al., "Spontaneous Nanoparticle Dispersal in Polybutadiene by Brush Forming End-Functional Polymers," *Macromolecules* 49, no. 4 (2016): 1434–1443, https://doi.org/10.1021/acs.macromol.5b02318.

34. M. K. Corbierre, N. S. Cameron, M. Sutton, K. Laaziri, and R. B. Lennox, "Gold Nanoparticle/Polymer Nanocomposites: Dispersion of Nanoparticles as a Function of Capping Agent Molecular Weight and Grafting Density," *Langmuir* 21, no. 13 (2005): 6063–6072, https://doi.org/10.1021/la047193e.

35. F. Foglia, Q. Berrod, A. J. Clancy, et al., "Disentangling Water, Ion and Polymer Dynamics in an Anion Exchange Membrane," *Nature Materials* 21, no. 5 (2022): 555–563.

36. W. Stöber, A. Fink, and E. Bohn, "Controlled Growth of Monodisperse Silica Spheres in the Micron Size Range," *Journal of Colloid and Interface Science* 26, no. 1 (1968): 62–69, https://doi.org/10.1016/0021-9797(68)90272-5.

37. S. Sun, Y. Lu, Z. Xu, et al., "Effect of Benzophenone Imine on Strain Softening Behavior of Natural Rubber/Carbon Black Nanocomposites," *Composites Part A: Applied Science and Manufacturing* 198 (2025): 109108, https://doi.org/10.1016/j.compositesa.2025.109108.

38. P. Kaur, L. Bowen, L. R. Hutchings, M. U. Chaudhry, T. Pugh, and R. L. Thompson, "Reinforcement of GO Composites Using Rigid and Flexible Crosslinkers," *Colloids and Surfaces A: Physicochemical and Engineering Aspects* 709 (2025): 136156, https://doi.org/10.1016/j.colsurfa.2025.136156.

39. H. T. Lim, K. H. Ahn, J. S. Hong, and K. Hyun, "Nonlinear Viscoelasticity of Polymer Nanocomposites Under Large Amplitude Oscillatory Shear Flow," *Journal of Rheology* 57, no. 3 (2013): 767–789.

40. T. Mezger, *The Rheological Handbook* (Vincentz Network, 2020).

41. C. P. Gibson, "Surface Modification of Hydrophobic Polymer Films With Amphiphilic Molecules," 2022 master's thesis, Durham University.

42. C. J. Carlile and M. A. Adams, "The Design of the IRIS Inelastic Neutron Spectrometer and Improvements to Its Analysers," *Physica B: Condensed Matter* 182, no. 4 (1992): 431–440, https://doi.org/10.1016/0921-4526(92)90047-V.

43. M. Appel, B. Frick, and A. Magerl, "A Flexible High Speed Pulse Chopper System for an Inverted Neutron Time-of-Flight Option on Backscattering Spectrometers," *Scientific Reports* 8, no. 1 (2018): 13580, https://doi.org/10.1038/s41598-018-31774-y.

44. D. Richard, M. Ferrand, and G. J. Kearley, "Analysis and Visualisation of Neutron-Scattering Data," *Journal of Neutron Research* 4, no. 1 (1996): 33–39, https://doi.org/10.1080/10238169608200065.

45. O. Arnold, J. C. Bilheux, J. M. Borreguero, et al., "Mantid–Data Analysis and Visualization Package for Neutron Scattering and SR Experiments," *Nuclear Instruments and Methods in Physics Research, Section A: Accelerators, Spectrometers, Detectors and Associated Equipment* 764 (2014): 156–166, https://doi.org/10.1016/j.nima.2014.07.029.

46. W. W. Young, R. Shi, X.-M. Jia, H.-J. Qian, and R. Katsumata, "Relating the Degree of Nanofiller Functionality to the Glass Transition Temperature and Structure in a Polymer–Polyhedral Oligomeric Silsesquioxane Nanocomposite," *Macromolecules* 55, no. 12 (2022): 4891–4898, https://doi.org/10.1021/acs.macromol.2c00646.

47. N. Makhiyanov and E. V. Temnikova, "The Glass-Transition Temperature and Structure of Amorphous Crystalline Butadiene Rubbers," *International Polymer Science and Technology* 39 (2012): 19–26.

48. V. Arrighi, J. Tanchawanich, and M. T. F. Telling, "Molar Mass Dependence of Polyethylene Chain Dynamics. A Quasi-Elastic Neutron Scattering Investigation," *Macromolecules* 46, no. 1 (2013): 216–225, https://doi.org/10.1021/ma301922j.

49. S. M. Kimani, R. L. Thompson, L. R. Hutchings, et al., "Multihydroxyl End Functional Polyethylenes: Synthesis, Bulk and Interfacial Properties of Polymer Surfactants," *Macromolecules* 47, no. 6 (2014): 2062–2071, https://doi.org/10.1021/ma402158b.

50. G. Arialdi, K. Karatasos, J. P. Rychaert, et al., "Local Dynamics of Polyethylene and Its Oligomers: A Molecular Dynamics Interpretation of the Incoherent Dynamic Structure Factor," *Macromolecules* 36 (2003): 8864–8875, https://doi.org/10.1021/ma0256789.

51. G. D. Smith and D. Bedrov, "A Molecular Dynamics Simulation Study of the α- and β-Relaxation Processes in 1,4-Polybutadiene," *Journal of Non-Crystalline Solids* 352, no. 42 (2006): 4690–4695, https://doi.org/10.1016/j.jnoncrysol.2006.02.142.

52. J. M. Hart, "The Study of Filled Rubber Composites With Rheology and Neutron Scattering," 2017 master's thesis, Durham University.

53. B. Yin, H. Wen, W. Luo, and M. Li, "Frequency- and Temperature-Dependent Payne Effect and Hysteresis Loss of Carbon Black Filled Rubbers: Experimental Study and Model Prediction," *Materials Today Communications* 33 (2022): 104920, https://doi.org/10.1016/j.mtcomm.2022.104920.

54. N. Warasitthinon, A.-C. Genix, M. Sztucki, J. Oberdisse, and C. G. Robertson, "The Payne Effect: Primarily Polymer-Related or

Filler-Related Phenomenon?,” *Rubber Chemistry and Technology* 92, no. 4 (2019): 599–611, https://doi.org/10.5254/rct.19.80441.

55. J. L. Keddie, R. A. L. Jones, and R. A. Cory, “Size-Dependent Depression of the Glass-Transition Temperature in Polymer-Films,” *Europhysics Letters* 27, no. 1 (1994): 59–64.

56. G. Kraus, “Mechanical Losses in Carbon-Black-Filled Rubbers,” *Journal of Applied Polymer Science* 39 (1984): 75–92.

57. A.-C. Genix, V. Bocharova, B. Carroll, et al., “How Tuning Interfaces Impacts the Dynamics and Structure of Polymer Nanocomposites Simultaneously,” *ACS Applied Materials & Interfaces* 15, no. 5 (2023): 7496–7510, https://doi.org/10.1021/acsami.2c18083.

58. F. T. Oyerokun and K. S. Schweizer, “Theory of Glassy Dynamics in Conformationally Anisotropic Polymer Systems,” *Journal of Chemical Physics* 123, no. 22 (2005): 224901, https://doi.org/10.1063/1.2135776.

59. M. Jhalaria, E. Buenning, Y. Huang, et al., “Accelerated Local Dynamics in Matrix-Free Polymer Grafted Nanoparticles,” *Physical Review Letters* 123, no. 15 (2019): 158003, https://doi.org/10.1103/PhysRevLett.123.158003.

Supporting Information

Additional supporting information can be found online in the Supporting Information section.